Lab on a Chip

Dynamic Article Links

Cite this: *Lab Chip*, 2011, **11**, 2929

www.rsc.org/loc

PAPER

Micro-valve using induced-charge electrokinetic motion of Janus particle

Yasaman Daghighi and Dongqing Li*

Received 14th March 2011, Accepted 9th June 2011
DOI: 10.1039/c1lc20229d

A new micro-valve using the electrokinetic motion of a Janus particle is introduced in this paper. A Janus particle with a conducting hemisphere and a non-conducting hemisphere is placed in a junction of several microchannels. Under an applied electric field, the induced-charge electrokinetic flow around the conducting side of the Janus particle forms vortices. The vortices push the particle moving forwards to block the entrance of a microchannel. By switching the direction of the applied electric field, the motion of the Janus particle can be changed to block different microchannels. This paper develops a theoretical model and conducts numerical simulations of the three-dimensional transient motion of the Janus particle. The results show that this Janus particle-based micro-valve is feasible for switching and controlling the flow rate in a microfluidic chip. This method is simple in comparison with other types of micro-valve methods. It is easy for fabrication, for operation control, and has a fast response time. To better understand the micro-valve functions, comparisons with a non-conducting particle and a fully conducting particle were made. Results proved that only a Janus particle can fulfill the requirements of such a micro-valve.

1. Introduction

The key microfluidic components are the micro-valves or micro-flow switches. They are used in order to develop fully integrated microfluidic chip devices, which can perform sequential loading and washing processes. While there is extensive research on micro-pumps and micro-mixers,[1–4] fewer advances were made in micro-flow valves.[5–9] Generally, micro-valves are categorized into two groups: (i) active and (ii) passive. In 1979, Terry *et al.*[10] introduced the first micro-valve. It was the first active magnetic micro-machined valve. After that, many others tried to make this type of micro-valve in different ways.[11–18] Among these magnetic micro-valves, pinch-type micro-valves became favourable because of their ability to provide zero leakage flow. Additionally, short response time, easy replacement of tubing, zero dead volume, and high flow range are the other advantages of these types of micro-valves. However, fabricating such micro-valves is difficult. Zdeblick and Angell introduced the first thermal micro-valve in 1987.[19] The function of these micro-valves is achieved by volumetric thermal expansion coupled with membrane deflection. Later, they used an actuator with a movable diaphragm in a sealed chamber, where the liquid or gas (or liquid–gas in two phases) was heated by the resistor built-in within the chamber.[20] This is the basis of most thermally actuated micro-valves. By using this actuated micro-valve technique, many others derived different types of thermal valves, such as: (i) thermo-pneumatic,[21–27] (ii) bimetallic,[28–33] and (iii) shape memory alloy.[34–36] The most important issues of the thermal micro-valves are the turn-on time (depending on the heat mass and the power of the heater) and the relaxation time (determined by the heat transfer to the external environment). As a result, the thermal micro-valve may have problems of operation control. Electrostatic micro-valves with flexible membranes have first been reported in 1994 by Sato and Shikida.[37,38] A few years later, another type of electrostatic valve was introduced which contained rigid silicon membranes.[39–45] High voltage is involved to operate this type of micro-valve. Since aqueous solutions electrolyse at high voltages, this type of micro-valve is suitable for a gas flow regulator, rather than liquid flow control. The development of new generations of micro-valves started around the year 2000 to overcome the drawbacks of the various MEMS-based micro-valves. Non-traditional micro-valves were invented such as phase change,[46–51] external pneumatic[52–56] or passive capillary micro-valves.[57–59]

Generally, there are many shortcomings and challenges associated with the existing micro-valves, which include: (i) complex fabrication and installation, (ii) moving parts, (iii) response time, (iv) resistible pressure, (v) leakage, (vi) dead volume, (vii) bulky external actuation means, (viii) bio-compatibility, and (ix) stability. In most cases, some form of external pump is required to drive the fluid. This means additional control issues and difficulties for miniaturization and integration. Improving any of these shortcomings will be a great step towards developing integrated microfluidic chips.

In this study, we introduce a novel micro-valve method which is based on controlling the induced-charge electrokinetic motion of a Janus particle. The proposed micro-valve is very simple. One

Department of Mechanical and Mechatronics Engineering, University of Waterloo, Waterloo, Ontario, Canada N2L 3G1. E-mail: dongqing@mme.uwaterloo.ca

Janus particle immersed in a micro-chamber, connecting several microchannels, will move by an externally applied electric field that controls the flow rate and flow direction. Three-dimensional numerical simulations were conducted to study the transient, induced-charge, electrokinetic motion of a Janus particle to see if this method would perform the function of the micro-valve. We also compared the effects of using a non-conducting particle and a fully conducting particle in the system. The results show that using these particles will cause leakage problems and instability. The range of the externally applied electric field for different flow rates in this micro-valve was also investigated.

2. Induced-charge electrokinetics (ICEK)

Once an external electric field E_e is applied, a fully conducting particle immersed in an aqueous solution will be induced to have surface charge.[60–64] Consequently, the counter-ions in the liquid are attracted by the induced surface charges. An induced dipolar electric double layer is thus formed (see Fig. 1).

Knowing the distribution of the ζ-potential of the induced electric double layer is necessary to calculate the velocity of the induced-charge electro-osmotic fluid flow around the conducting particle and electrophoretic motion of the particle. A numerical technique capable of calculating the induced ζ-potential was proposed by Wu and Li.[60–63] This method is summarized as follows.

At steady state, the strength of the local induced charge field E_i of the conducting surface is the same as the externally applied electrical field E_e but in the opposite direction,

$$|E_i| = |E_e| \text{ or } E_i = -E_e \tag{1}$$

Since $\vec{E} = -\nabla\phi_e$, the above equation can be written in the following form

$$\nabla\zeta_i = -\nabla\phi_e \tag{2}$$

If a fully conducting particle is initially electrically neutral, the integration of the induced charge and hence the induced ζ-potential over the conducting surface should be zero, that is

$$\oint_S \zeta_i \, ds = 0 \tag{3}$$

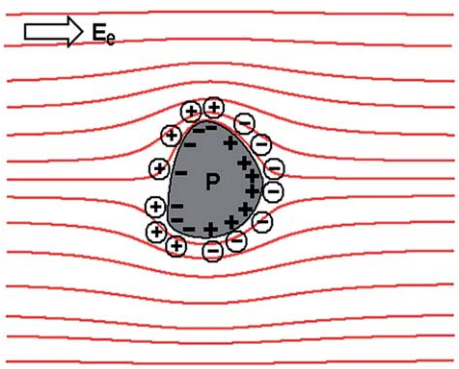

Fig. 1 Steady-state electric field and the induced dipolar electric double layer around a fully conducting object in an aqueous solution.

where S is the conducting surface under the applied electric field. If there is initial electrostatic charge on the surface, superposition of the initial ζ-potential $\zeta_0 = \zeta(t = 0)$ and the induced ζ-potential ζ_i will give the total ζ-potential distribution.

From eqn (2), the following equation can be used to determine the distribution of the induced ζ-potential on the conducting surfaces

$$\zeta_i = -\phi_e + \phi_c \tag{4}$$

where ϕ_c is a constant. By inserting eqn (4) into eqn (3), ϕ_c can be calculated by:

$$\phi_c = \frac{\int_S \phi_e dA}{A} \tag{5}$$

where A is the area of the entire surface of the conducting object. Employing the above equations allows a simple numerical method to calculate the final steady state induced ζ-potential distribution on the conducting surfaces of arbitrary geometries.

The "Janus Particle" here means one type of heterogeneous particle, half of it is electrically conducting and the other half is electrically non-conducting. In this study, we consider a spherical Janus particle, a half of it is metal (the conducting half) and another half is polymer (the non-conducting half), as illustrated in Fig. 2. For such a Janus particle, the electro-osmotic slip velocity on the non-conducting hemisphere is given by the Holmholtz–Smoluchowski equation[65]

$$\vec{u} = -\frac{\varepsilon_w \zeta}{\mu}\vec{E}_e \tag{6a}$$

where ζ, ε_w and μ are the constant ζ-potential at the non-conducting surface, the dielectric constant and the viscosity of the liquid, respectively. The Holmholtz–Smoluchowski equation[65] can be used for calculating the slip velocity on the conducting surface of the Janus particle similarly. However, on the conducting part, the ζ-potential is the induced ζ-potential, ζ_i,

$$\vec{u}_i = -\frac{\varepsilon_w \zeta_i}{\mu}\vec{E}_e \tag{6b}$$

The strategy of Wu and Li[60] is employed to calculate the induced-charge ζ-potential on the polarisable portion of the Janus particle. The induced ζ-potential is a function of the local applied electric field, $\zeta_i = f(\vec{E}_e)$. The induced-ζ-potential varies in different positions on the conducting surface. Consequently, the

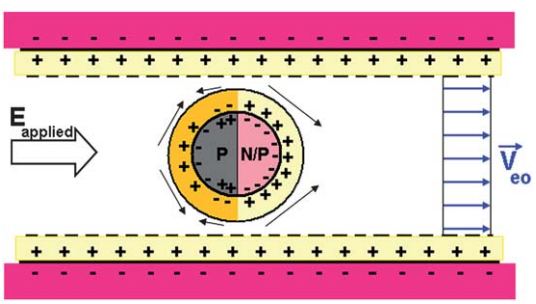

Fig. 2 The electro-osmotic flow around a Janus particle in a straight microchannel. The arrows represent the direction of electro-osmotic velocity of the flow on different sections of the particle surface.

velocity of the electro-osmotic flow changes over the polarisable part of the particle. On the other hand, the slip velocity on the non-conducting part of the Janus particle may be in a different direction from that of the conducting part. As a result of these variations, different vortices in opposite directions will be generated near the solid–liquid interface of the Janus particle (see Fig. 2). More detailed discussions about vortex formation around the Janus particle can be found elsewhere.[64]

3. Three dimensional governing equations

The interactions of the applied electric field with the induced surface charge on the conducting part of the particle and with the electrostatic charge on the non-conducting part of the particle will create the electrophoretic motion of the particle. The interaction of the applied electric field with the electrostatic charges on the non-conducting microchannel also causes electro-osmotic flow (EOF) in the channel. The net velocity of the particle will be determined by the electrophoretic motion of the particle, the bulk liquid EOF and the complex flow field (vortices) around the particle. The list of assumptions inherent in the system of equations is provided in Table 1. A complete 3-D transient mathematical model is set up to simulate the electric field, the flow field and the particle motion in a microchannel, as described in the following sections.

3.1. Electric field

In order to solve the Laplace's equation ($\nabla^2\phi_e = 0$) and find out the applied electrical potential ϕ_e in the liquid, we assumed: (i) the conducting part of the Janus particle is completely polarized and (ii) a steady state induced dipolar electric double layer is set up on the conducting surface. The corresponding boundary conditions in this case are

$$\vec{n}\cdot\nabla\phi = 0 \text{ at channel wall and particle surface} \quad (7a)$$

$$\phi = \phi_0 \text{ at channel inlet} \quad (7b)$$

$$\phi = 0 \text{ at channel outlet} \quad (7c)$$

Table 1 The list of assumption used in the modeling and simulation

Assumptions
The initial polarization process is fast enough to be neglected.
The steady state condition is valid for induced charge polarisable particle.
The externally applied electric field is DC and constant.
The fully conducting part of the particle is initially electrically neutral.
The Debye length is negligible (in comparison with the size of the particle and the size of the channel).
Slipping flow boundary condition is valid based on thin EDL.
The Holmholtz–Smoluchowski equation can be used for calculating the slip velocity.
The non-conducting part of the particle is electrostatically charged.
Laplace's equation ($\nabla^2\phi_e = 0$) is valid in this study.
The liquid in the microchannel is considered as a Newtonian incompressible liquid.

3.2. Flow field

The liquid in the microchannel is considered as a Newtonian incompressible flow. The continuity equation

$$\nabla\ \vec{u} = 0 \quad (8)$$

and the Navier–Stokes equation

$$\rho\left[\frac{\partial\ \vec{u}}{\partial t} + \vec{u}\nabla\ \vec{u}\right] = -\nabla p + \mu\nabla^2\ \vec{u} \quad (9)$$

are the governing equations with the boundary conditions of[66–68]

$$\vec{u} = -\frac{\varepsilon_0\varepsilon\zeta_w}{\mu}\vec{E} \text{ and } \vec{n}\nabla p = 0 \quad \text{at the channel wall} \quad (10a)$$

$$\vec{u} = \vec{V}_p + \vec{\omega}_p \times \left(\vec{x}_p - \vec{X}_p\right) - \frac{\varepsilon_0\varepsilon\zeta_p}{\mu}\vec{E} \text{ and } \vec{n}.\nabla p = 0 \text{ at the particle surface} \quad (10b)$$

$$\vec{n}\cdot\nabla\ \vec{u} = 0 \text{ and } p = P_a \quad \text{at the inlet and outlet} \quad (10c)$$

$\vec{E} = -\nabla\phi_e$ is the local applied electric field. ζ_w is the ζ-potential on the channel wall, while ζ_p is the ζ-potential on the particle surface (*i.e.*, it is the induced ζ-potential on the conducting part, and the electrostatic charge caused ζ-potential on the non-conducting part). $\vec{V}_p$ and $\vec{\omega}_p$ are the translational and the rotational velocity of the particle respectively. The position vector of the particle surface and the position vector of the particle center are correspondingly represented by $\vec{x}_p$ and $\vec{X}_p$. Since the system is physically time-dependent the transient term in eqn (9), $\partial\ \vec{u}/\partial t$, cannot be dropped off.

The bulk liquid flow influences the particle's motion and the particle's motion will also affect the flow field. Thus, a fully coupled transient particle–fluid interaction strategy is required to solve such a problem which is the current method.

3.3. Particle motion

Electrostatic force is exerted on the particle. This force is applied by the external electric field. On the other hand, the flow field applies a hydrodynamic force on the particle. The net force acting on the particle is given by[66–68]

$$\vec{F}_{net} = \vec{F}_h + \vec{F}_E \quad (11)$$

where F_h is the total hydrodynamic force and F_E is the electrostatic force. The hydrodynamic force includes two components:

$$\vec{F}_h = \vec{F}_{h\_out} + \vec{F}_{h\_in} \quad (12)$$

where $\vec{F}_{h\_out}$ and $\vec{F}_{h\_in}$ represent the hydrodynamic force acting on the particle by the liquid flow in the region outside and inside the EDL (electric double layer). In the current study the Debye length is assumed negligible (in comparison with the size of the particle and the size of the channel) since we assumed that the electrical double layers are so thin. In this way the flow field around the particles is the flow field originated outside the EDL and subject to the slipping flow boundary condition at the particle surface. Under this assumption, it can be shown that the F_E is balanced by $\vec{F}_{h\_out}$, and the net force on the particle is thus given by[66–68]

$$\vec{F}_{\text{net}} = \vec{F}_{\text{h\_out}} = \vec{G} - \oint_{\Gamma} \sigma_{\text{P}} . \vec{n} \mathrm{d}S = (\rho - \rho_{\text{P}}) g \forall_{\text{P}} - \oint_{\Gamma} \sigma_{\text{P}} . \vec{n} \mathrm{d}S \quad (13)$$

where $\vec{G}$ is the total body force, $\forall_{\text{P}}$ is the volume of the particle, ρ_{p} is the density of the particle, g is the acceleration due to gravity. The total torque acting on the particle is given by

$$T_{\text{net}} = -\oint_{\Gamma} (\vec{x}_{\text{p}} - \vec{X}_{\text{p}}) \times (\sigma_{\text{P}} \cdot \vec{n}) \mathrm{d}S \quad (14)$$

σ_{p} is the stress tensor given by

$$\sigma_{\text{p}} = -p\bar{\bar{I}} + \mu \left[(\nabla \vec{u}) + (\nabla \vec{u})^{T} \right] \quad (15)$$

where $\bar{\bar{I}}$ is the identity tensor.

The equations governing the particle motion are based on the Newton's second law:

$$m_{\text{p}} \frac{\mathrm{d}\vec{V}_{\text{p}}}{\mathrm{d}t} = \vec{F}_{\text{net}} \quad (16)$$

$$J_{\text{p}} \frac{\mathrm{d}\vec{\omega}_{\text{p}}}{\mathrm{d}t} = \vec{T}_{\text{net}} \quad (17)$$

where m_{p} and J_{p} are the mass and the moment of inertia of the particle, respectively. The displacement of the particle center is governed by

$$\frac{\mathrm{d}\vec{X}_{\text{p}}}{\mathrm{d}t} = \vec{V}_{\text{p}} \quad (18)$$

The initial conditions of the particle motion and the flow velocity are set as zero, that is

$$\vec{V}_{\text{p}}|_{t=0} = 0, \quad \vec{\omega}_{\text{p}}|_{t=0} = 0 \text{ and } \vec{u}|_{t=0} = 0 \quad (19)$$

In the development of the numerical simulation, the following non-dimensionalized parameters were used:

$$\overline{\phi}_{\text{e}} = \frac{\phi_{\text{e}}}{\zeta_{\text{w}}}, \ \overline{\vec{u}} = \frac{\vec{u}}{U_{\text{ref}}}, \ \overline{\vec{x}} = \frac{\vec{x}}{d}, \ \bar{t} = \frac{t}{d/U_{\text{ref}}},$$

$$\overline{P} = \frac{p - P_{\text{a}}}{\rho U_{\text{ref}}^{2}}, \ \overline{\vec{E}} = \frac{\vec{E}}{\zeta_{\text{w}}/d}$$

where $U_{\text{ref}} = \frac{\varepsilon\varepsilon_0}{\mu} \frac{\zeta_{\text{w}}}{d}$ is the reference velocity.

4. Geometry and computational domain

In this study, the micro-valve includes (i) one cylindrical microchamber connecting to (ii) three microchannels of a circular cross-section, (iii) one spherical Janus particle, and (iv) four electrodes, as illustrated in Fig. 3a. The microchannels are named as A to C for more convenience when they are referred in the following sections of this paper. The basic function of the valve is to block one of the two outlets at a given time, while letting the liquid flow through the other outlet. This function is then achieved by moving the Janus particle to block the desired outlet. The motion of a spherical Janus particle initially placed at the center of the microvalve is studied by a three dimensional numerical simulation. This 3D numerical simulation is based on the mathematical model described above. The diameter of the Janus particle is considered as D_{p}. To achieve the full blockage, the diameter of all microchannels is chosen to be smaller than the diameter of the Janus particle. The diameter of microchannel A is 75% of D_{p}. The diameter of the other two microchannels is chosen to be half of D_{p}. In the computation domain (Fig. 3), all the microchannels' lengths are equal to D_{p}. The diameter and height of the microchamber are chosen to be two times bigger than the Janus particle diameter to let the Janus particle move freely in the microchamber.

The channel walls as well as the non-conducting surface of the Janus particle carry uniform negative electric charges that are

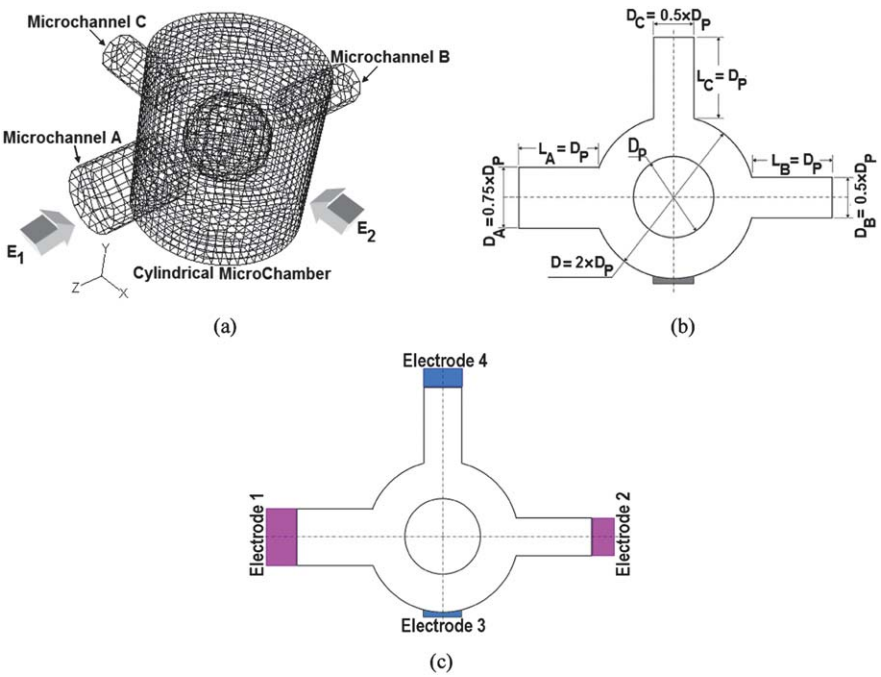

Fig. 3 Schematic diagram of the micro-valve with three microchannels and one suspended Janus particle in it. (a) Computational domain. E_1 and E_2 represent the external electric field directions. (b) Geometry and dimensions in non-dimensional format. (c) The location of electrodes.

characterized by the ζ-potentials. The ζ-potentials on the non-conducting surface of the particle is −50 mV; and −15 mV on the channel walls. The density of the particle is assumed to be the same as the liquid in order to avoid the gravity effect. Four electrodes are placed to provide the driving forces in the system, as shown in Fig. 3c. Applying voltage between electrodes 1 and 2 produces a potential difference and generates an electric field which is called E_1 in this study. Electrodes 3 and 4 can be used to produce an electric field, named E_2. The applied electric fields can be set as any desired values. The liquid flow in this system is entirely driven by electro-osmosis. The ends of the microchannels are connected to open reservoirs, so that no overall pressure gradient is present in the system.

With respect to the fabrication, the proposed valve can be made by the alignment methods and the methods which are used to develop microchannels with a circular cross-section. There are different applicable methods to produce various shapes for microchannel cross-sections. Fabrication of a microchannel with star grooves, rhombus grooves,[69] and with cylindrical shape[70–72] is already reported. Thus, a cylindrical cross-section for the microvalve chamber and the microchannels is a realistic design. To make a microfluidic chip which includes different sections, where some of them are not at the same level as the others, the alignment method plays a significant role. Over the years, great effort has been made to improve the alignment efficiency.[73–75] Hence, the proposed microchannel structure can be made by existing fabrication methods.

The computational domain is fully covered by 3D meshes. In order to display the system clearly, the number of meshes are reduced in Fig. 3. Using the coarse meshes in Fig. 3a facilitates visualization of the particle (suspended inside of the microchamber) and microchannels. It should be noted that the presented results in this paper are based on the mesh independent study. The mathematical models in the computation domain were solved by commercial software FLUENT 12 which, in correlation with visual C, runs a UDF file that was written for solving the moving mesh and particle motion in 3D. The physical properties for the fluid and the specifications for the microchannel used in the simulations are shown in Table 2.

5. Results and discussion

5.1. Alignment of a Janus particle with the applied electric field

Under the applied electric field, the conducting part of the Janus particle is induced to have an electric charge. The induced charge will interact with the applied electric field. A Janus particle is unaligned when the normal vector at the interface of its two hemispheres has an angle with the applied electric field. An unaligned Janus particle under the applied electric field will rotate to line up itself with the applied electric field due to the electric field force. During alignment, the induced charge will change while the orientation of the particle changes. Consequently the induced-charge electrokinetic flow field around the Janus particle also changes. To understand this process better,

Table 2 Constants used in the numerical simulations

Parameters	Values
Dielectric constant, ε	80
Permittivity of vacuum, ε_0 (C V^{-1} m^{-1})	8.854×10^{-12}
Viscosity, μ (kg m^{-1} s^{-1})	0.9×10^{-3}
Density, ρ (kg m^{-3})	998
ζ-Potential on channel walls (mV)	−50
ζ-Potential on non-conducting hemisphere of Janus particle (mV)	−15
Particle diameter, D	D_1
Diameter of microchannel A, D_A	$0.75 \times D_p$
Diameter of microchannel B and C, D_B, D_C	$0.5 \times D_p$
Length of microchannels, L_A, L_B, L_C	D_p
Diameter of microchamber, D_{ch}	$2 \times D_p$
Height of microchamber, H_{ch}	$2 \times D_p$

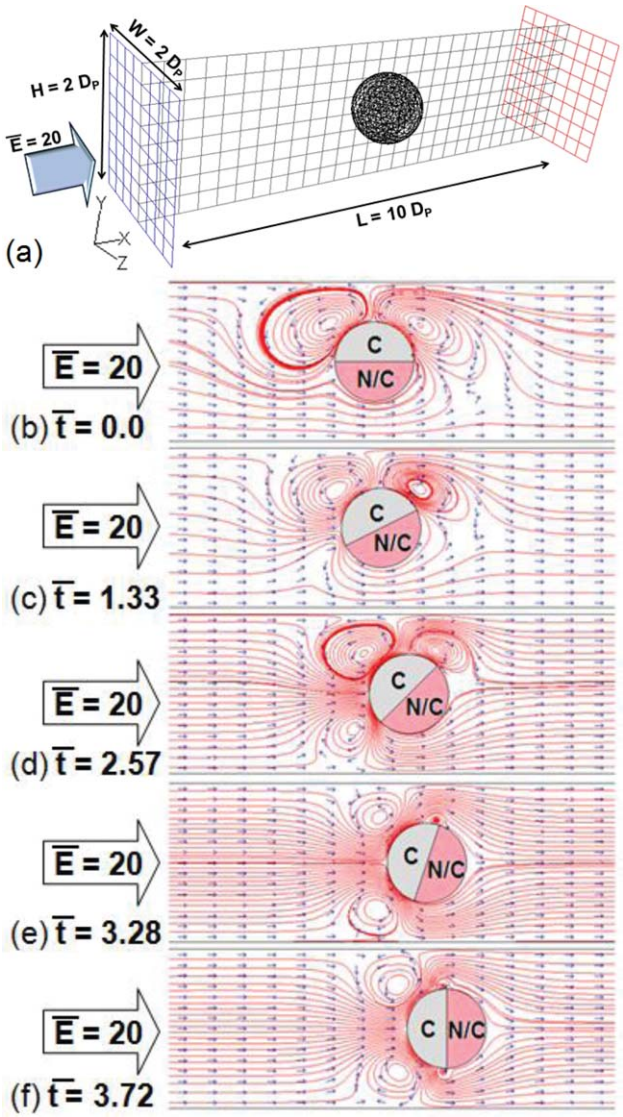

Fig. 4 An example of the transient rotational and translational motion of a Janus particle in a straight microchannel. (a) The results are represented in the x–y plane crossing the 3D straight microchannel (b) The translational and rotational motion of the Janus particle under applied external electric field in different time steps. The streamlines are plotted to show the flow field in the microchannel around the Janus particle. The arrows indicate the flow direction. The length of microchannel is $L = 10D_p$ and the size of the channel cross-section is $W = H = 2D_p$. Non-dimensionalized external applied electric field is 20 when the zeta potential on the non-conductive surface of Janus particle and also the channel wall is −50 mV. The Janus particle diameter is considered as D_p. "C" represents the conducting material, while the non-conducting material is represented by "N/C" in this figure.

consider a Janus particle immersed in an aqueous solution, in a straight microchannel. The normal vector of the Janus particle at the interface of its two hemispheres has a 90° angle with the applied electric field. The conducting half faces the top wall of the microchannel, as shown in Fig. 4b. Once the electric field is applied, the electro-osmotic flow passes the non-conducting section of the Janus particle smoothly, while two vortices are formed around the conducting section. For such a Janus particle, the conducting section has an induced dipolar EDL, a portion with positive charge and a portion with negative charge in the induced EDL, as illustrated in Fig. 2. This dipolar EDL is responsible for the two vortices on the conducting side. The externally applied field exerts a body force on the excess counter-ions in the EDL region of the liquid. This force moves the liquid, but because the sign of the surface charge (hence the excess counter ions in the induced EDL) changes from one part to another part of the conducting section, the direction of liquid flow varies and becomes opposite to each other. Consequently two vortices around the conducting section are generated. As seen from Fig. 4, the size and the position of the vortices change as the particle rotates. The creation of the vortices is because the local electric field on the conducting surface changes. Consequently, the induced dipolar EDL also changes. Eventually, the Janus particle reaches its stable position (does not rotate any longer) when the conducting hemisphere faces the applied electric field.

5.2. Micro-valve using the Janus particle

The basic function of the valve is to block one of the two outlets at a given time, while letting the liquid flow through the other outlet. This function is achieved by moving the Janus particle to block the desired outlet. Fig. 5 shows the numerical simulation of the valve operation. Here we assume the Janus particle is initially located in the center of the valve chamber with the conducting side facing the microchannel A. Once the external electric field, E_1, is applied, the vortices generate on the conducting side of the Janus particle and push the Janus particle to move towards the

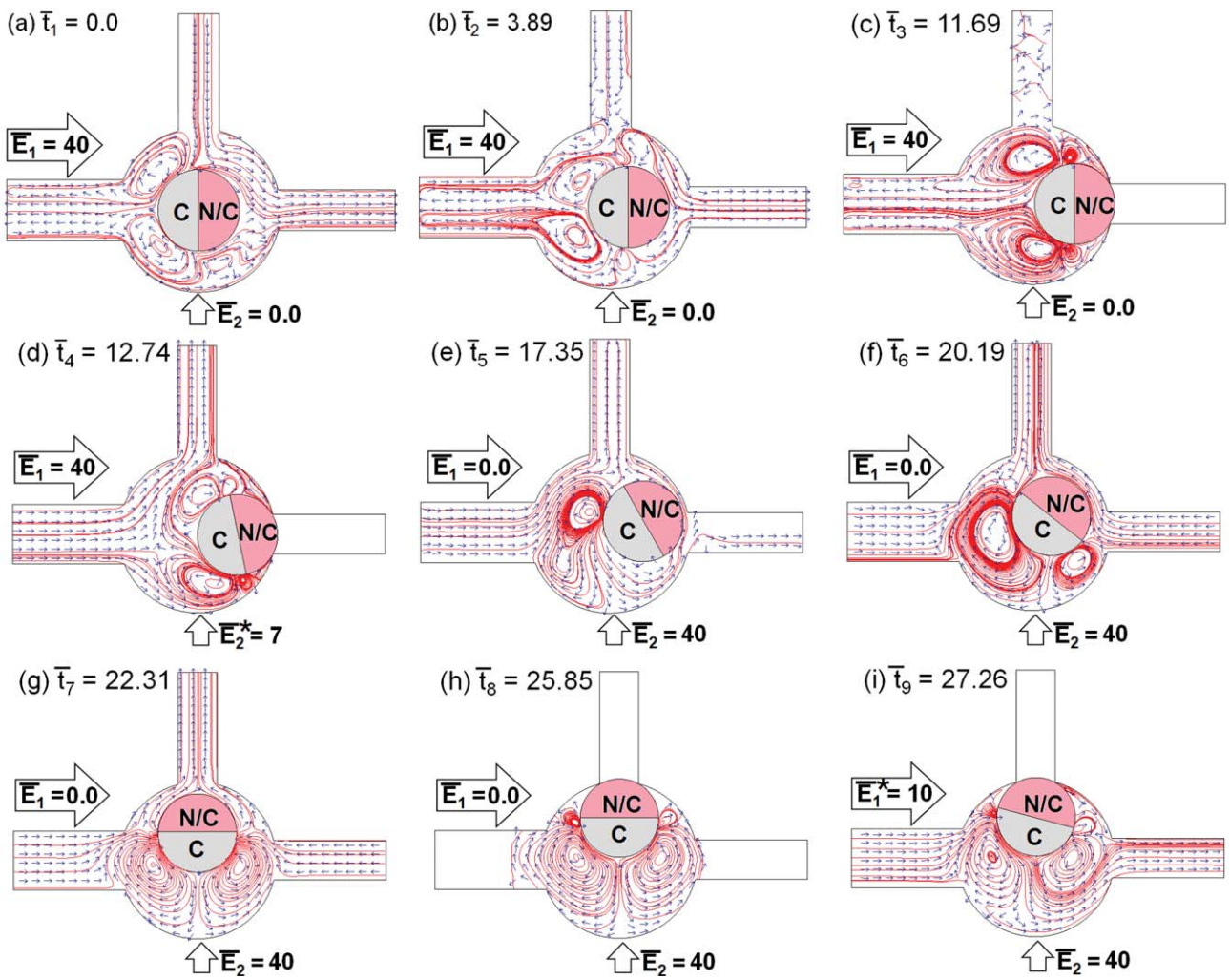

Fig. 5 The switching process of the micro-valve operation controlled by the induced-charge electrokinetic motion of a Janus particle. The streamlines are plotted to show the flow field in the microchannel around the Janus particle. The arrows indicate the flow direction. The results represent the x–z plane crossing the middle of the 3D microvalve at different time steps. $\bar{E}_1$, $\bar{E}_1^*$, $\bar{E}_2$, $\bar{E}_2^*$ are the non-dimensionalized external applied electric field when the zeta potential on the channel wall is ¬50 mV. The Janus particle diameter is considered as D_p. "C" represents the conducting material, while the non-conducting material is represented by "N/C" in this figure.

microchannel B (see Fig. 5a and b). After approximately $\Delta\bar{t} = 11.69$ the Janus particle reaches the entrance of the horizontal outlet and blocks it (Fig. 5c). The Janus particle is two times bigger than the outlet and is capable of blocking the outlet completely as long as the external electric field is applied. At this stage, in order to drive liquid flow through the microchannel C, another external electric field is applied, $\bar{E}_2^* = 35$ V cm^{-1}, while the electric field $\bar{E}_1$ remains unchanged. $\bar{E}_2^*$ is sufficiently weaker than $\bar{E}_1$ so that it will not break the blocking of the microchannel B while generating electro-osmotic flow to the microchannel C (see Fig. 5d). Because of the two electric fields, the Janus particle rotates slightly at the same position to align itself with the resultant electric field. In the next step, we changed the flow direction by opening the microchannel B and blocking the microchannel C. To achieve this goal, we turned off the $\bar{E}_1$ electric field, and increase the $\bar{E}_2$ electric field to 40. As a result, the Janus particle rotates to align itself with the new electric field and moves towards the microchannel C and eventually blocks it (Fig. 5e–h). Under the specified electric field, this process takes approximately $\Delta\bar{t} = 13.11$. Consider case A when the diameter of the microchamber is considered as $D_{ch} = 2D_p = 40$ μm, and during the switching process $E_1 = E_2 = 200$ V cm^{-1}, $E_1^* = 50$ V cm^{-1}, $E_2^* = 35$ V cm^{-1}. In this case the non-dimensionalized electric field respectively becomes $\bar{E}_1 = 40$, $\bar{E}_2 = 40$, $\bar{E}_1^* = 10$, $\bar{E}_2^* = 7$. In this case the switching process is the period that particle moves from the entrance of microchannel B (Fig. 5d) and reaches the entrance of microchannel C (Fig. 5h). This period for the presented case A will take $\Delta\bar{t} = 3.7$s which can be written as $\Delta\bar{t} = 13.11$ in non-dimensional format. At this step, there is no liquid flow through any of the microchannels. In order to have liquid flow to the microchannel B, we applied a weaker external electric field in the desired direction, $\bar{E}_1^* = 10$. The Janus particle rotates itself to align with the new resultant electric field while keeping its blocking position. In this way, the microchannel C is completely blocked, the liquid flow direction switched to a new path, from left inlet to the right outlet (see Fig. 5i).

As shown in Fig. 5, by turning on the electric field $\bar{E}_1$, the dominant flow direction is from the left (microchannel A) to the right (microchannel B). As the Janus particle gets close to the entrance of the microchannel B, the flow rate in the left-to-right direction decreases. Consequently, less and less liquid will be drawn into the valve chamber from the microchannel C (Fig. 5b). Fig. 5c shows that there is no flow in the microchannel B as it is blocked by the Janus particle, and no flow in the microchannel C since there is no electro-osmotic force to drive the liquid to that direction. When an additional electric field, $\bar{E}_2^*$, is turned on, while the microchannel B is still blocked, the liquid is forced to flow from the microchannel A to the only open microchannel C. Blocking one channel and diverting the liquid to another channel is the main goal of the valve, this function is achieved at this stage. Next, turning on $\bar{E}_2$ as the dominant electric field, while $\bar{E}_1$ is turned off, causes the Janus particle to rotate and to align itself with the electric field direction (as shown in Fig. 5e–h). When the Janus particle (under the effect of the new electric field) rotates and leaves the entrance of the microchannel B, the liquid gets permission to enter or exit that gate. Since the electric field force at this moment is in a direction to push the liquid to the microchannel C, the liquid will be drawn from both microchannels A and B (according to the continuity law) into the chamber, as shown in Fig. 5e–g. The suction power is directly related to the dominant flow rate. As the Janus particle moves towards the microchannel C and eventually blocks the path, the main flow rate reduces. As a result, the flow from the microchannels A and B also becomes smaller. When the Janus particle completely blocks the microchannel C, and the only applied electric field is $\bar{E}_2$, there is no electro-osmotic flow into or out of the two open microchannels. However the existing electric field induces the electric charge on the conducting section of the particle, and the induced charge produces vortices in the remaining liquid in the microchamber (Fig. 5h). Finally, turning on the electric field, $\bar{E}_1^*$ (to a value sufficiently smaller than $\bar{E}_2$), will produce an electro-osmotic flow from channel A to channel B, while keeping the microchannel C in a completely blocked state (Fig. 5i). In Fig. 5 the velocity vector arrows' size is normalized to visualize the flow direction better. However, the size of the arrows does not represent the strength of velocity vectors.

Totally, switching the flow outlet takes approximately $\Delta\bar{t} = 13.11$, under a maximum electric field of $\bar{E}_2^* = 40$. When a more powerful electric field is applied, the valve's switching can be shorter. For example, the time required for the switching is $\Delta\bar{t} = 8.14$ when $\bar{E}_2^* = 80$ is applied. Considering case A, we can say that the switching process takes approximately $\Delta t = 3.7$ s, under a maximum electric field of $E_2^* = 200$ V cm^{-1}. This switching value will be shorter ($\Delta t = 2.3$ s) when the applied electric field is $E_2^* = 400$ V cm^{-1}. Fig. 6 shows the dependence of the valve switching time on the external electric field strength. Clearly, increasing the electric field decreases the required switching time.

As discussed above, when an outlet is blocked, an additional weaker electric field is used to pump the liquid out of the opening outlet. This pumping electric field can be changed within a range so that it can adjust the flow rate of the liquid pumped out of the valve, without affecting the blocking position of the Janus particle. In the case of Fig. 5d, the dominant electric field is $\bar{E}_1 = 40$ and the pumping electric field, can vary from $\bar{E}_2^* = 5.8$ V cm^{-1} to 9.2 V cm^{-1}. In the case of Fig. 5i, the dominant electric field is $\bar{E}_2 = 40$ V cm^{-1} and the pumping electric field can vary from $\bar{E}_1^* = 9.8$ to 14.6.

When the particle moves close to the microchamber wall, the non-uniformity of the electric field in the gap between the non-conducting part of the particle and the microchamber wall produces dielectrophoresis (DEP) force on the particle and affects the particle motion. According to the theory of

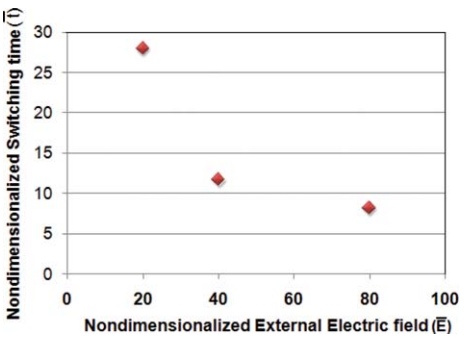

Fig. 6 The relation of the valve switching time to the external applied electric field in the normal dimensionalized format.

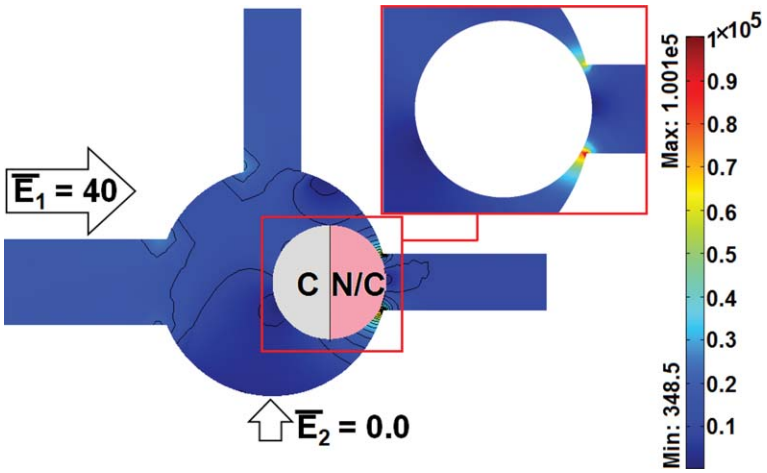

Fig. 7 The electric field distribution in the microchamber when the particle is very close to the microchannel B. The electric field contours and the electric field distribution near to the particle (zoom in). $\bar{E}_1$, $\bar{E}_2$ are the non-dimensionalized external applied electric field when the zeta potential on the channel wall is −50 mV. The Janus particle diameter is considered as D_p. "C" represents the conducting material, while the non-conducting material is represented by "N/C" in this figure.

dielectrophoresis (DEP), under a DC field, the DEP force is a negative force that will push the particle towards the lower electric field.

For a spherical particle with a diameter of D_P under a DC electric filed, the DEP force exerting on this particle is given by:

$$F_{DEP} = -\pi\varepsilon\left(\frac{D_p}{2}\right)^3 \nabla|\vec{E}|^2 \qquad (20)$$

The non-uniform electric field in the gap region can be calculated numerically. For a spherical non-conducting particle with a diameter of $D_p = 20$ μm at the position as shown in Fig. 7, the DEP force is equal to 50.2×10^{-23} N. Its direction is from right to left.

When the Janus particle is in the position as shown in Fig. 7, the other forces acting on the particle (except DEP force) can be calculated numerically as well. These forces are generated by electroosmosis, electrophoresis and the vortices around the particle. If we call the summation of these forces as the applied force, $F_{applied}$, and calculate it numerically, the result is $F_{applied} = 39.8 \times 10^{-19}$ N. Its direction is from left to right. Among these

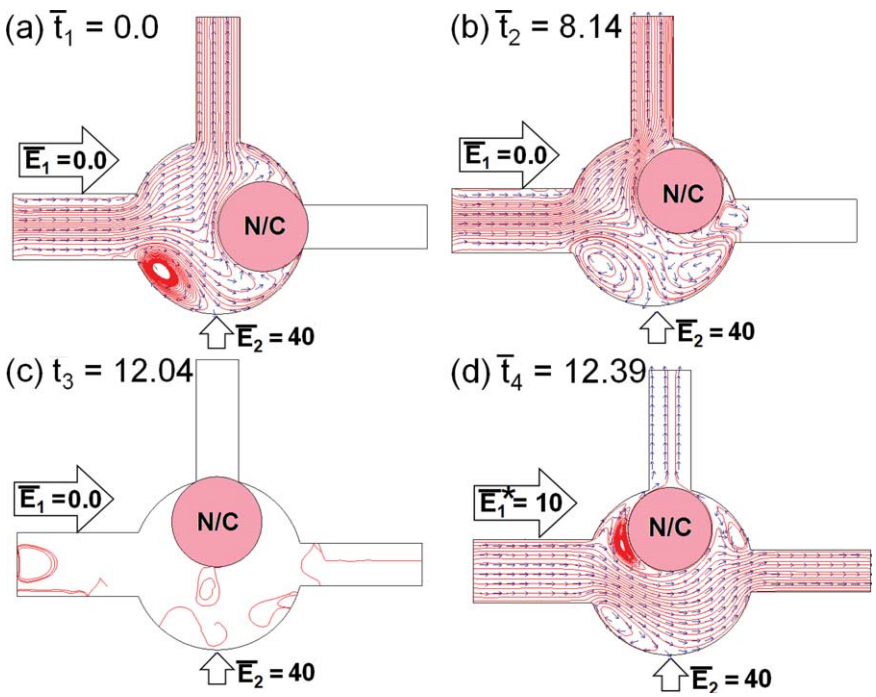

Fig. 8 The switching process of the micro-valve using a non-conducting particle. The streamlines are plotted to show the flow field in the microchannel around the Janus particle. The arrows indicate the flow direction. The results represent the *x*–*z* plane crossing the middle of the 3D micro-valve at different time steps. $\bar{E}_1^*$, $\bar{E}_2$ are the non-dimensionalized external applied electric field when the zeta potential on the channel wall is −50 mV. The non-conducting material is represented by "N/C" in this figure.

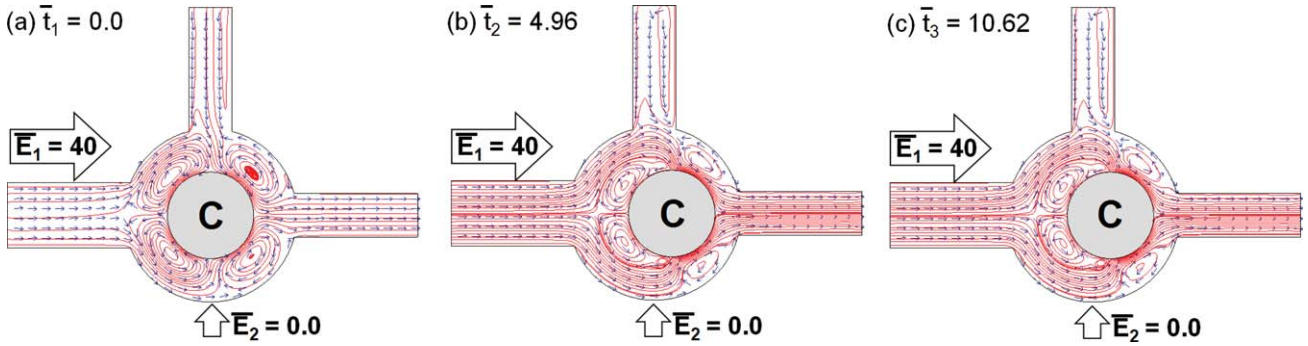

Fig. 9 The switching process of the micro-valve using a fully conducting particle The streamlines are plotted to show the flow field in the microchannel around the Janus particle. The arrows indicate the flow direction. The results represent the x–z plane crossing the middle of the 3D micro-valve at different time steps. E1, E2 are the non-dimensionalized external applied field when the zeta potential on the channel wall is −50 mV. The Janus particle diameter is considered as D_p. "C" represents the conducting material.

force components, the vortices around the conducting section of the Janus particle produce a strong force on the particle.

Comparing $F_{applied}$ of the Janus particle and F_{DEP} of a sphere non-conducting particle demonstrates that the $F_{applied}$ by far is the dominant force. The applied force is much (four order of magnitude) bigger than the DEP force. Thus, the dielectrophoresis (DEP) force is not considered in the simulation of the Janus particle in this study.

5.3. Micro-valve using a non-conducting particle

The possibilities of using a non-conducting particle or a fully conducting particle to realize the function of such a micro-valve were also investigated. Fig. 8 shows a micro-valve with a non-conducting particle. Consider the switching process from blocking the horizontal outlet to blocking the vertical outlet. Once we set $\bar{E}_1 = 0$ and $\bar{E}_2 = 40$, the non-conducting particle moves with the streamlines and follows the micro-chamber wall to reach the microchannel C. This switching process takes about 3.5 s which is shorter than the micro-valve with the Janus particle. However, a problem occurred when we turned on the weaker pumping electric field, $\bar{E}_1^* = 10$, to generate flow to the microchannel B. Once E_1* is applied, the non-conducting particle starts to leave its blocking position as shown in Fig. 8d. As long as the pumping electric field E_1 exists, the non-conducting particle will keep moving toward the right side as time passes. This results in leakage from the vertical outlet. Therefore, using a non-conducting particle in the present micro-valve design does not satisfy the requirements.

Comparing the stage as shown in Fig. 8d with the equivalent stage of the Janus particle (Fig. 5i), one can see that in Fig. 5i, the charges generate two vortices in the liquid in the microchamber, and the vortices keep the particle in the blocking position while the electroosmotic pumping from A to B is in operation. However, in the case of a non-conducting particle, as shown in Fig. 8d, there are no vortices to hold the particle to block the channel C. When the additional electric field, E_1^*, is turned on to drive the liquid to flow from channel A to channel B, the force resulted from the combined electric field, both E_1 and E_2, will push the non-conducting particle to leave the entrance of the microchannel C.

Considering the DEP force in the case of the non-conducting particle leads to an increase in the switch time. Since there are no vortices acting on the particle, calculations can show that the DEP force will be comparable with the net force arising from electro-osmotic and electrophoretic effects. Therefore, the DEP force will prevent the non-conducting particle from getting very close to the entrance of microchannel C.

5.4. Micro-valve using a fully conducting particle

Fig. 9 shows what happens when a fully conducting particle is placed in the micro-valve. Four vortices generate around the conducting particle when the external electric field is applied. The fully conducting particle initially moves from the center of the chamber to the downstream of the flow but eventually stops, and cannot reach the horizontal outlet. As the particle gets closer to the right side wall, the two vortices in the downstream of the particle (on the right hand side of the particle) interact with the wall. When the motion of the rotating liquid is restricted by the solid wall, the momentum of the liquid motion converts to pressure, which results in a repellent force between the wall and the particle and pushes the fully conducting particle away from the wall, and hence prevents the particle from blocking the entrance of the microchannel B. Therefore, using a fully conducting particle cannot achieve the valve's function.

6. Concluding remarks

A novel micro-valve is introduced in this paper. This micro-valve is very simple and operates by controlling the induced-charge electrokinetic motion of a Janus particle inside a micro-chamber by applied electric field. It is shown that the orientation of the Janus particle is sensitive to the direction of the applied electric field. By switching the direction of a main electric field, the Janus particle can quickly block or open the outlet of the micro-valve. The flow rate through the micro-valve can be controlled by applying another electric field for pumping. Increasing the main electric field can decrease the switching time of the valve. It is demonstrated that both non-conducting and fully conducting particles cannot be used to achieve the valve function, because the non-conducting particle has the leakage problem and the fully conducting particle cannot block the outlet. The proposed

micro-valve using a Janus particle has great potential for developing integrated microfluidic lab-on-a-chip devices.

Nomenclatures

E_e	an external electric field
E_i	local induced charge field of the conducting surface
ϕ_e	applied electrical potential
ϕ_c	constant electrical potential
$\vec{u}$	electro-osmotic slip velocity on the non-conducting surface
$\vec{u}_i$	electro-osmotic slip velocity on the conducting surface
$\vec{V}_p$	translational velocity of the particle
$\vec{\omega}_p$	rotational velocity of the particle
$\forall_P$	volume of the particle
S	conducting surface
A	area of the entire surface of the conducting object
$\vec{G}$	total body force
μ	viscosity of the liquid
ρ	liquid density
ρ_p	density of the particle
$\vec{F}_{net}$	the net force acting on the particle
$\vec{F}_h$	total hydrodynamic force
$\vec{F}_E$	electrostatic force
$\vec{F}_{h\_out}$	hydrodynamic force acting on the particle by the liquid flow in the region outside the EDL
$\vec{F}_{h\_in}$	hydrodynamic force acting on the particle by the liquid flow in the region inside the EDL
T_{net}	total torque acting on the particle
EDL	electric double layer
T_e	Maxwell stress tensor
ζ	ζ-potential
ζ_i	induced ζ-potential
ζ_0	initial ζ-potential
ζ_w	ζ-potential on the channel wall
ζ_p	ζ-potential on the particle surface
ε_w	dielectric constant
$\vec{x}_p$	position vector on the particle surface
$\vec{X}_p$	position vector of the particle center
g	acceleration due to gravity.
$\overline{\overline{I}}$	identity tensor
σ_p	stress tensor
m_p	mass of inertia of the particle
J_p	moment of inertia of the particle
U_{ref}	reference velocity
P	pressure
$\vec{\overline{E}} = \frac{\vec{E}}{\zeta_w/d}$	non-dimensionalized external electric field
$\overline{\phi}_e = \frac{\phi_e}{\zeta_w}$	non-dimensionalized electric potential
$\vec{\overline{x}} = \frac{\vec{x}}{d}$	non-dimensionalized position
$\overline{t} = \frac{t}{d/U_{ref}}$	non-dimensionalized time
$\overline{P} = \frac{p - P_a}{\rho U_{ref}^2}$	non-dimensionalized pressure
$\vec{\overline{u}} = \frac{\vec{u}}{U_{ref}}$	non-dimensionalized velocity
DEP	dielectrophoresis

Acknowledgements

The authors wish to thank the financial support of the Canada Research Chair program and the Natural Sciences and Engineering Research Council (NSERC) of Canada through a research grant to D. Li.

References

1 D. J. Laser and J. G. Santiago, A review of micropumps, *J. Micromech. Microeng.*, 2004, **14**, R35–R64.
2 C. K. Fredrickson and Z. H. Fan, Macro-to-micro interfaces for microfluidic devices, *Lab Chip*, 2004, **4**, 526–533.
3 N.-T. Nguyen and Z. Wu, Micromixers—a review, *J. Micromech. Microeng.*, 2005, **15**, R1–R6.
4 V. Hessel, H. Löwe and F. Schönfeld, Micromixers—a review on passive and active mixing principles, *Chem. Eng. Sci.*, 2005, **60**(8), 2479–2501.
5 K. W. Oh and C. H. Ahn, A review of microvalves, *J. Micromech. Microeng.*, 2006, **16**, R13–R39.
6 C. Zhang, D. Xing and Y. Li, Micropumps, microvalves and micromixers within PCR microfluidic chips: advantages and trends, *Biotechnol. Adv.*, 2007, **25**, 483–514.
7 G. Simone, G. Perozziello, G. Sardella, I. Disegna, S. Tori, N. Manaresi and G. Medoro, A microvalve for hybrid microfluidic systems, *Microsyst. Technol.*, 2010, **16**(7), 1269–1276.
8 J. Casals-Terré, M. Duch, J. A. Plaza, J. Esteve, R. Pérez-Castillejos, E. Vallés and E. Gómez, Design, fabrication and characterization of an externally actuated ON/OFF microvalve, *Sens. Actuators, A*, 2008, **147**(2), 600–606.
9 J. Liu, C.-F. Chen, S. Yang, C.-C. Chang and D. L. Devoe, Mixed-mode electrokinetic and chromatographic peptide separations in a microvalve-integrated polymer chip, *Lab Chip*, August 2010, **10** (16), 2122–2129.
10 S. C. Terry, J. H. Jerman and J. B. Angell, A gas chromatographic air analyzer fabricated on a silicon wafer, *IEEE Trans. Electron Devices*, 1979, **26**, 1880–1886.
11 K. Yanagisawa, H. Kuwano and A. Tapo, An Electromagnetically Driven Microvalve, in *Proc. Transducers'93*, 1993, pp. 102–105.
12 O. Krusemark, A. Feustel and J. Muller, Micro Ball Valve for Fluidic Micropumps and Gases, *Proc. Micro Total Analysis Systems '98 Workshop*, 1998, pp. 399–402.
13 A. Meckes, J. Behrens, O. Kayser, W. Benecke, T. Becker and G. Muller, Microfluidic system for the integration and cyclic operation of gas sensors, *Sens. Actuators, A*, 1999, **76**, 478–483.
14 H. J. Cho, K. W. Oh, C. H. Ahn, P. Boolchand and T.-C. Nam, Stress analysis of silicon membranes with electroplated permalloy films using Raman scattering, *IEEE Trans. Magn.*, 2001, **37**, 2749–2751.
15 K. W. Oh, R. Rong and C. H. Ahn, In-line Micro Ball Valve through Polymer Tubing, in *Proc. MicroTAS 2001*, 2001, pp. 407–408.
16 B. Bae, N. Kim, H. Kee, S.-H. Kim, Y. Lee, S. Lee and K. Park, Feasibility test of an electromagnetically driven valve actuator for glaucoma treatment, *J. Microelectromech. Syst.*, 2002, **11**, 344–354.
17 C. Fu, Z. Rummler and W. Chomburg, Magnetically driven micro ball valves fabricated by multilayer adhesive film bonding, *J. Micromech. Microeng.*, 2003, **13**, S96–S102.
18 K. W. Oh, R. Rong and C. H. Ahn, Miniaturization of pinch-type valves and pumps for practical micro total analysis system integration, *J. Micromech. Microeng.*, 2005, **15**, 2449–2455.

19 M. J. Zdeblick and J. B. Angell, A Microminiature Electric-to-fluidic Valve, in *The 4th International Conference on Solid-State Sensors and Actuators (Transducers '87)*, Tokyo, Japan, June 1987, pp. 827–9.
20 M. J. Zdeblick, R. Anderson, J. Jankowski, B. Kline-Schoder, L. Christel and R. Miles, et al., Thermopneumatically Actuated Microvalves and Integrated Electro-fluidic Circuits, in *Technical Digest of the Solid-State Sensor and Actuator Workshop*, Hilton Head, South Carolina, USA, June 13–16, 1994, p. 251–255.
21 A. Ruzzu, K. Bade, J. Fahrenberg and D. Maas, Positioning system for catheter tips based on an active microvalve system, *J. Micromech. Microeng.*, 1998, **8**, 161–164.
22 C.-M. Ho, X. Yang, C. Grosjean and Y.-C. Tai, A MEMS thermopneumatic silicone rubber membrane valve, *Sens. Actuators, A*, 1998, **64**, 101–108.
23 X. Yang, C. Grosjean and Y.-C. Tai, Design, fabrication, and testing of micromachined silicone rubber membrane valves, *J. Microelectromech. Syst.*, 1999, **8**, 393–402.
24 D. Baechi, R. Buser and J. Dual, A high density microchannel network with integrated valves and photodiodes, *Sens. Actuators, A*, 2002, **95**, 77–83.
25 C. A. Rich and K. D. Wise, A high-flow thermopneumatic microvalve with improved efficiency and integrated state sensing, *J. Microelectromech. Syst.*, 2003, **12**, 201–208.
26 J.-H. Kim, K.-H. Na, C. J. Kang, D. Jeon and Y.-S. Kim, A disposable thermopneumatic-actuated microvalve stacked with PDMS layers and ITO-coated glass, *Microelectron. Eng.*, 2004, **73–74**, 864–869.
27 H. Takao, K. Miyamura, H. Ebi, M. Ashiki, K. Sawada and K. Ishida, A MEMS microvalve with PDMS diaphragm and two-chamber configuration of thermo-pneumatic actuator for integrated blood test system on silicon, *Sens. Actuators, A*, 2005, **119**, 468–475.
28 H. Jerman, Electrically activated, normally closed diaphragm valves, *J. Micromech. Microeng.*, 1994, **4**, 210–216.
29 P. W. Barth, Silicon Microvalves for Gas Flow Control, in *Proc. 8th Int. Conf. on Solid-State Sensors and Actuators (Transducers '95)*, 1995, pp. 276–277.
30 R. H. Wolf and A. H. Heuer, TiNi (shape memory) films on silicon for MEMS applications, *J. Microelectromech. Syst.*, 1995, **4**, 206–212.
31 D. Reynaerts, J. Peirs and H. Van Brussel, An implantable drug-delivery system based on shape memory alloy micro-actuaries, *Sens. Actuators, A*, 1997, **61**, 455–462.
32 M. Kohl, D. Dittmann, E. Quandt and B. Winzek, Thin film shape memory microvalves with adjustable operation temperature, *Sens. Actuators, A*, 2000, **83**, 214–219.
33 Y. Liu, M. Kohl, K. Okutsu and S. Miyazaki, A TiNiPd thin film microvalve for high temperature applications, *Mater. Sci. Eng., A*, 2004, **378**, 205–209.
34 C. M. Pemble and B. C. Towe, A miniature shape memory alloy pinch valve, *Sens. Actuators, A*, 1999, **77**, 145–148.
35 M. Kohl, D. Dittmann, E. Quandt, B. Winzek, S. Miyazaki and D. M. Allen, Shape memory microvalves based on thin films or rolled sheets, *Mater. Sci. Eng., A*, 1999, **273–5**, 784–788.
36 C. R. Tamanaha, L. J. Whitman and R. J. Colton, Hybrid macro–micro fluidics system for a chip-based biosensor, *J. Micromech. Microeng.*, 2002, **12**, N7–N17.
37 K. Sato and M. Shikida, An electrostatically actuated gas valve with an S-shaped film element, *J. Micromech. Microeng.*, 1994, **4**, 205–209.
38 M. Shikida, K. Sato, S. Tanaka, Y. Kawamura and Y. Fujisaki, Electrostatically driven gas valve with high conductance, *J. Microelectromech. Syst.*, 1994, **3**, 76–80.
39 A. H. Epstein, et al., Power MEMS and Microengines, in *Proc. IEEE Conf on Solid State Sensors and Actuators (Transducer '97)*, 1997, pp. 753–756.
40 J. K. Robertson and K. D. Wise, A low pressure micromachined flow modulator, *Sens. Actuators, A*, 1998, **71**, 98–106.
41 L. Yobas, M. A. Huff, F. J. Lisy and D. M. Durand, A novel bulk micromachined electrostatic microvalve with a curved-compliant structure applicable for a pneumatic tactile display, *J. Microelectromech. Syst.*, 2001, **10**, 187–196.
42 J. Schaible, J. Vollmer, R. Zengerle, H. Sandmaier and T. Strobelt, Electrostatic Microvalves in Silicon with 2-way Function for Industrial Applications, in *11th Int. Conf. on Solid-State Sensors and Actuators (Transducers '01)*, 2001, pp. 928–31.
43 W. Van der Wijngaart, H. Ask, P. Enoksson and G. Stemme, A high-stroke, high-pressure electrostatic actuator for valve applications, *Sens. Actuators, A*, 2002, **100**, 264–271.
44 L. Yobas, D. M. Durand, G. G. Skebe, F. J. Lisy and M. A. Huff, A novel integrable microvalve for refreshable Braille display system, *J. Microelectromech. Syst.*, 2003, **12**, 252–263.
45 M. M. Teymoori and E. Abbaspour-Sani, Design and simulation of a novel electrostatic peristaltic micromachined pump for drug delivery applications, *Sens. Actuators, A*, 2005, **117**, 222–229.
46 D. J. Beebe, J. S. Moore, J. M. Bauer, Q. Yu, R. H. Liu, C. Devadoss and B. H. Jo, Functional hydrogel structures for autonomous flow control inside microfluidic channels, *Nature*, 2000, **404**, 588–590.
47 Y. Liu, C. B. Rauch, R. L. Stevens, R. Lenigk, J. Yang, D. B. Rhine and P. Grodzinski, DNA amplification and hybridization assays in integrated plastic monolithic devices, *Anal. Chem.*, 2002, **74**, 3063–3070.
48 L. Klintberg, M. Karlsson, L. Stenmark, J. A. Schweitz and G. Thornell, A large stroke, High force paraffin phase transition actuator, *Sensors Actuators A*, 2002, **96**, 189–195.
49 E. T. Carlen and C. H. Mastrangelo, Surface micromachined paraffin-actuated microvalve, *J. Microelectromech. Syst.*, 2002, **11**, 408–420.
50 P. Selvaganapathy, E. T. Carlen and C. H. Mastrangelo, Electrothermally actuated inline microfluidic valve, *Sens. Actuators, A*, 2003, **104**, 275–282.
51 R. H. Liu, J. Yang, R. Lenigk, J. Bonanno and P. Grodzinski, Self-contained, fully integrated biochip for sample preparation, polymerase chain reaction amplification, and DNA microarray detection, *Anal. Chem.*, 2004, **76**, 1824–1831.
52 M. A. Unger, H.-P. Chou, T. Thorsen, A. Scherer and S. R. Quake, Monolithic microfabricated valves and pumps by multilayer soft lithography, *Science*, 2000, **288**, 113–116.
53 H. Takao, M. Ishida and K. Sawada, A pneumatically actuated full in-channel microvalve with MOSFET-like function in fluid channel networks, *J. Microelectromech. Syst.*, 2002, **11**, 421–426.
54 Y.-C. Wang, M. H. Choi and J. Han, Two-dimensional protein separation with advanced sample and buffer isolation using microfluidic valves, *Anal. Chem.*, 2004, **76**, 4426–4431.
55 K. W. Oh, C. Park and K. Namkoong, A World-to-chip Microfluidic Interconnection Technology with Dual Functions of Sample Injection and Sealing for a Multichamber Micro PCR Chip, in *Proc. IEEE MEMS*, 2005, pp. 714–717.
56 A. Wego, S. Richter and L. Pagel, Fluidic Microsystems based on printed circuit board technology, *J. Micromech. Microeng.*, 2001, **11**, 528–531.
57 S. Santra, P. Holloway and C. D. Batich, Fabrication and testing of a magnetically actuated micropump, *Sens. Actuators, B*, 2002, **87**, 358–364.
58 S. Chung, J. K. Kim, K. C. Wang, D.-C. Han and J.-K. Chang, Development of MEMS-based cerebrospinal fluid shunt system, *Biomed. Microdevices*, 2003, **5**, 311–321.
59 G.-H. Feng and E. S. Kim, Micropump based on PZT unimorph and one-way parylene valves, *J. Micromech. Microeng.*, 2004, **14**, 429–435.
60 Z. Wu and D. Li, Micromixing using induced-charge electrokinetic flow, *Electrochim. Acta*, 2008, **53**, 5827–5835.
61 Z. Wu and D. Li, Mixing and flow regulating by induced-charge electrokinetic flow in a microchannel with a pair of conducting triangle hurdles, *Microfluid. Nanofluid.*, 2008, **5**, 65–76.
62 Z. Wu and D. Li, Induced-charge electrophoretic motion of ideally polarizable particles, *Electrochim. Acta*, 2009, **54**, 3960–3967.
63 Z. Wu, Y. Gao and D. Li, Electrophoretic motion of ideally polarized particles in microchannels, *Electrophoresis*, 2009, **30**, 773–781.
64 Y. Daghighi, Y. Gao and D. Li, 3D numerical study of induced-charge electrokinetic motion of a heterogeneous particle in a microchannel, *Electrochim. Acta*, 2011, **56**, 4254–4262.
65 J. N. Anker, C. J. Behrend, H. Huang and R. Kopelman, *J. Magn. Magn. Mater.*, 2005, **293**, 655.
66 C. Ye and D. Li, *J. Colloid Interface Sci.*, 2004, **272**, 480–488.
67 C. Ye and D. Li, Eccentric electrophoretic motion of a spherical particle in a circular cylindrical microchannel, *Microfluid. Nanofluid.*, 2005, **1**, 234–241.
68 C. Ye and D. Li, Electrophoretic motion of two particles in a rectangular microchannel, *Microfluid. Nanofluid.*, 2004, **1**, 52–61.
69 S.-W. Kang and D. Huang, Fabrication of star grooves and rhombus grooves micro heat pipe, *J. Micromech. Microeng.*, 2002, **12**, 525–531.

70 l.-j. Yang, Y.-T. Chen, S.-W. Kang and Y.-C. Wang, Fabrication of SU-8 embedded microchannels with circular cross-section, *Int. J. Mach. Tool Manufact.*, 2004, **44**, 1109–1114.
71 V. Maselli, R. Osellame, G. Cerullo, R. Ramponi, P. Laporta, L. Magagnin and P. L. Cavallotti, Fabrication of long microchannels with circular cross section using astigmatically shaped femtosecond laser pulses and chemical etching, *Appl. Phys. Lett.*, 2006, **88**, 191107.
72 S.-H. Song, C.-K. Lee, T.-J. Kim, I.-C. Shin, S.-C. Jun and H.-I. Jung, A rapid and simple fabrication method for 3-dimensional circular microfluidic channel using metal wire removal process, *Microfluid. Nanofluid.*, 2010, **9**, 533–540.
73 R. Yang, S. A. Soper and W. Wang, Microfabrication of pre-aligned fiber bundle couplers using ultraviolet lithography of SU-8, *Sens. Actuators, A*, 2006, **127**(1), 123–130.
74 D. E. Lee, S. Soper and W. Wang, Design and fabrication of an electrochemically actuated microvalve, *Microsyst. Technol.*, 2008, **14**, 1751–1756.
75 K.-H. Jeong and L. P. Lee, A novel microfabrication of a self-aligned vertical comb drive on a single SOI wafer for optical MEMS applications, *J. Micromech. Microeng.*, 2005, **15**, 277–281.

